On a Discrete Element Method to simulate the mechanical behavior of heterogeneous media

W. LECLERC[a], H. HADDAD[b], M. GUESSASMA[a], J. FORTIN[a]

a. Université de Picardie Jules Verne, LTI, EA 3899, 02100 Saint Quentin, France
willy.leclerc@u-picardie.fr, mohamed.guessasma@u-picardie.fr, jerome.fortin@u-picardie.fr
b. Centre européen de la céramique, SPCTS, CNRS 7315, 87068 Limoges, France.

Résumé :

La présente contribution est dédiée à la simulation mécanique de milieux hétérogènes continus par une méthode d'éléments discrets cohésifs. Dans cette approche, nous considérons un modèle équivalent au continu basé sur des empilements de disques en 2D ou de sphères en 3D. La cohésion est introduite à l'échelle des particules où les liaisons de contact avec les particules avoisinantes sont remplacées par des poutres décrites par le modèle d'Euler-Bernoulli. En outre, un processus de calibration doit être mis en place afin de relier les propriétés locales au comportement mécanique effectif. Des études sont réalisées sur plusieurs microstructures, à savoir des problèmes à inclusion seule et un matériau plus complexe pour lequel un volume élémentaire représentatif est généré. Des comparaisons sont réalisées avec la méthode des éléments finis lesquelles montrent la pertinence de l'approche discrète. Dans un second temps, la décohésion interfacielle et un critère de rupture basé sur la contrainte hydrostatique sont pris en compte dans le modèle. L'influence de la microstructure sur l'initiation et la propagation de fissures est alors étudiée dans le cadre d'un composite renforcé en fibres unidirectionnelles.

Abstract :

The present work is dedicated to the mechanical simulation of continuous and heterogeneous media using a cohesive discrete element method. In this approach, an equivalent continuous model based on granular packings composed of disks in 2D and spheres in 3D is considered. The cohesion is introduced at the scale of particles by replacing the contact links by beam elements described by Euler-Bernoulli theory. Before starting any calculations, a calibration process is set up to relate the mechanical properties of beam elements to the effective ones. Investigations are performed on several microstructures, namely single inclusion problems and a more complex material for which a representative volume element is generated. Comparisons are done with the finite element method which exhibit the consistency of the discrete approach. In a second step, the interfacial debonding and a failure criterion based on the hydrostatic stress are taken into account. Cracks initiation and propagation are investigated in the framework of a multi-fiber composite.

Key Words : Discrete Element Method, Numerical Simulation, Beam Elements, Elastic Properties, Cracks Propagation

1 Introduction

The numerical prediction of mechanical behavior of materials is an interesting tool for industrialists and others desiring to invest in new materials with superior properties without costly experimental appliances. However, the case of composite materials leads to the issue of the validity of the numerical simulation. In fact, due to a potentially complex microstructure and several phenomena among them the interfacial debonding, the variability of properties in a given phase and the presence of local defects and cracks, the numerical measure is often quite far from the experimental one. Thus, a suitable and reliable numerical approach able to reproduce the geometry of the microstructure as well as the scope of phenomena arising at different scales of the medium is required. Introduced in the seventies in the framework of rock mechanics [1, 2], the Discrete Element Method (DEM) has been described as numerically costly and poorly efficient during a long time and restricted to specific fields. Today, the access to more powerful numerical resources, the parallel computing and the development of coupling methods [3, 4] give to such an approach a second birth. Thus, the DEM is, among others, seen as an interesting alternative to more classical approaches such as the Finite Element Method (FEM). The DEM is a flexible numerical tool able to more naturally treat damaging and contact effects whatever the heterogeneity of the medium. Besides, the method enables to take into account multi-scale effects since it intrinsically introduces a variability of properties at the scale of the particle.

In the last decade, numerous works discussed the simulation of continuous media and its damaging using a Discrete Element (DE) approach [5, 6]. The most important issue was to define cohesion laws to precisely model the continuity of the material. Thus, pioneering works of Schlangen [7] described the cohesion using beam elements introduced between each pair of particles in contact within a granular packing fitting the computational domain. The author exhibited that beam elements provide more realistic crack patterns than spring ones under various mechanical loadings. More recently, André et al. [8] considered a hybrid particulate-lattice model using the same paradigm and proved that that the DEM is a relevant approach to quantitatively yield the linear elastic behavior of homogeneous continuous media. However, it was verified that such a result is only true when a set of intrinsic geometrical parameters related to granular packings such as the compacity and the coordination number are perfectly monitored. In fact, such an approach is greatly sensitive to the arrangement of granular packings as established in the works of Kumar et al. [9]. More recently, other works explored the issue of the mechanical behavior of heterogeneous media. Thus, Haddad et al. [10] investigated the definition of the stress tensor in heterogeneous media in the context of a 2D random particulate composite and Maheo et al. [11, 12] investigated the case of a 3D unidirectional fiber composite.

The present work is a contribution aiming to investigate the relevance of the DEM to simulate the mechanical behavior of heterogeneous media and its damaging. In order to model the continuous medium, granular packings composed of disks in 2D or spheres in 3D are generated using the efficient Lubachevsky-Stillinger Algorithm (LSA) [13]. Thus, under several assumptions related to the spatial arrangement of particles and the concept of Random Close Packing (RCP) [14], this is qualified as isotropic and supposed representative of the continuous domain. The cohesion between particles is then introduced by beam elements the description of which is based on Euler-Bernoulli theory in which torsion, tensile and bending terms are taken into account. The main idea is that each link of the initial network of contact forces is replaced by a cohesive beam element the properties of which have to be correlated to the expected macroscopic properties of the medium. From a practical standpoint, a calibration process is carried out and charts are used to relate microscopic and macroscopic mechanical behaviors.

The outline of the paper is as follows. In a first section, we introduce and describe the concept of Equivalent Continuous Domain (ECD) the assumptions of which ensure the isotropy of the granular system and prevent all arrangement effects. The calibration process is described and charts are given in the example of 3D granular systems. The second section is dedicated to the investigation of heterogeneous media, namely single inclusion problems and the case of a multi-fiber composite. Comparisons are done with the Finite Element Method in terms of stress field dtermined using Zhou's formulation [15] at the scale of the particle and using Love-Weber formulation [16, 17] at a mesoscale introduced with the help of a tessellation of the domain in specimen [10, 16]. The third section described the application to cracks initiation and propagation in the example of the multi-fiber composite. For that purpose, we consider a failure criterion based on the Removed Discrete Element Failure (RDEF) process introduced by André et al. [18] and interfacial debonding using the Discrete Damage Zone Model (DDZM) initially introduced by Liu et al. [19] for FEM. The last section presents some conclusions and prospects.

2 Numerical model

2.1 Equivalent Continuous Domain

The first step of the DEM-based approach consists in discretizing the continuous domain at the macroscopic scale by a granular packing composed of disks in 2D or spheres in 3D. Under several assumptions of polydispersity, orientation and size, the granular domain can be considered as an Equivalent Continuous Domain (ECD) in that this is enough representative of the continuous medium. First, the compacity has to meet the assumption of RCP which is characterized by a compacity close to 85% for a network of disks in 2D and 64% for a network of spheres in 3D. Second, the coordination number which represents the average number of particles in contact with one given particle has to be controlled, namely close to 4.5 in 2D, and 6.2 in 3D. Third, a slight polydispersity of particle size must be introduced in order to avoid undesirable directional effects. Typically, the particle's radius follows a Gaussian distribution law and the dispersion is characterized by the coefficient of variation which is set to 0.3 in the present work. These characteristics ensure the randomness of the granular packing and consequently the isotropy of the ECD. For information purposes, the efficient LSA is used in the present work to generate granular packings under these assumptions. Moreover, similarly to the discretization of an FE mesh, the density of the granular packing has to be accurately estimated in order to avoid a bias in mechanical calculations based on DEM. In a final optional step, the network of contacts is densified using a Delaunay triangulation process applied from this initial cloud of particle's centers with respect to the initial network. Such a process leads to about 10% additional contacts and provides in the same time a Voronoï tessellation and areas of representation for each particle and its contacts.

2.2 Calibration process

The cohesive link between two particles is modeled by a beam element the intrinsic parameters of which are the length L_μ, the Young's modulus E_μ, the cross-section A_μ and the quadratic moment I_μ (see Figure 2). Practically speaking, A_μ and I_μ are related to a dimensionless parameter $\mathrm{r}_\mu \in]0, 1]$ which reads :

$$\mathrm{r}_\mu = \frac{2\mathrm{a}_\mu}{\mathrm{R}_i + \mathrm{R}_j} \tag{1}$$

where a_μ is the height of a rectangular cross section in 2D and the radius of a circular cross section in 3D, and R_i and R_j are respectively the radius of a pair of particles in contact i and j. Thus, the mechanical

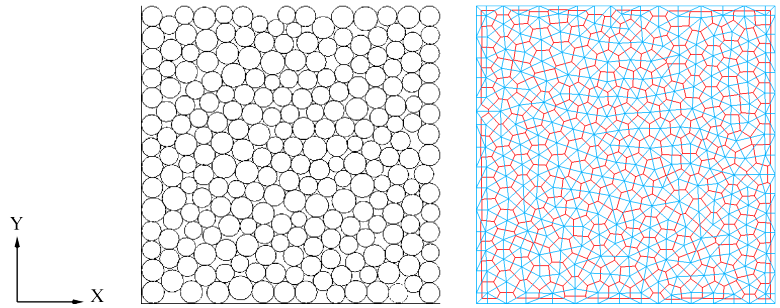

Figure 1: Example of a typical 2D Voronoï construction based on a granular packing constituted of 200 particles: (a) granular packing and (b) corresponding Voronoï tessellation

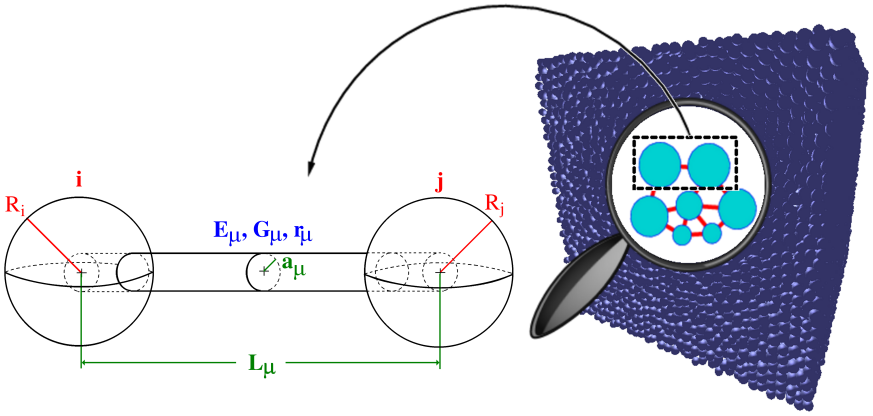

Figure 2: Cohesive beam model

behavior of the beam is described by the only parameters E_μ, r_μ and the size of particles which is directly connected to the density of the packing. Preliminary studies exhibited that a minimum of 7000 particles in 2D and 700,000 particles in 3D has to be considered to prevent all discretization effects. The main issue is that on the contrary of FE calculations for which local properties at the scale of the element are identical to the macroscopic properties for a homogeneous material, microscopic properties of the beam element (E_μ, r_μ) have to be correlated to macroscopic mechanical properties as done in several previous works. Typically, quasi-static tensile and shear tests are performed and macroscopic elastic properties (E_M, ν_M) are extracted from numerical calculations for a given pair of parameters (E_μ, r_μ). The process is repeated for a full range of investigated configurations so that the evolution of microscopic properties enables to choose the desired macroscopic ones. Figures 3a and b illustrate the influence of r_μ parameter on the non-dimensional Young's modulus E^a, which is the ratio between the macroscopic Young's modulus E_M and the microscopic one E_μ, and the Poisson's ratio ν_M. Please notice that calibration curves are given for 3D simulations without Delaunay triangulation step, and 2D simulations lead to qualitatively similar results.

3 Elastic behavior of heterogeneous media

3.1 Single inclusion problems

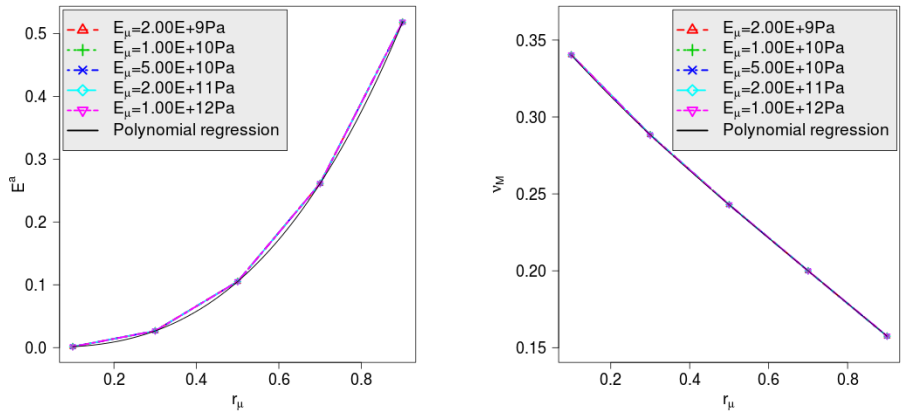

Figure 3: Influence of r_μ parameter on (a) the non-dimensional Young's modulus E^a and (b) the Poisson's ratio ν_M

3.1.1 Spherical inclusion problem

We study the case of a 3D heterogeneous medium composed of a metallic spherical inclusion embedded in a ceramic matrix. The elastic properties of the inclusion are as follows. The macroscopic Young's modulus E^i_M is 72.5 GPa and the Poisson's ratio is 0.33. The corresponding microscopic Young's modulus E^i_μ is 12,020 GPa and the r^f_μ parameter is 0.169. The matrix phase is composed of ceramic material of macroscopic Young's modulus E^m_M 350 GPa and Poisson's ratio 0.24. The corresponding microscopic Young's modulus E^m_μ is 2,536 GPa and the r^m_μ parameter is 0.545. Please notice that the microscopic Young's modulus E^Γ_μ of beam elements connecting two particles belonging to two different phases throughout the interface Γ between the matrix and the fiber is given by the geometric average of microscopic Young's moduli. The heterogeneous medium is modeled using a cubic pattern of length L=1cm composed of a centered spherical inclusion. The radius of the sphere is equal to L/3 so that the volume fraction of the sphere ϕ_S is theoretically equal to 0.155. Practically, each particle is associated to a given phase according to the position of its center and ϕ_S is estimated by summing the volume of each particle located within the inclusion and dividing the result by the contributions of all particles. Thus, the result is very sensitive to the density of granular packing and mainly affected by two phenomena, the wall effects and the irregularities arising at the interface between the matrix and the inclusion. Preliminary tests led us to choose a total number of 2,000,000 particles to ensure an error threshold of 1% with respect to the theoretical value.

We consider the framework of a quasi-static tensile test with symmetric boundary conditions and an imposed velocity of $1e^{-5}$ m/s. Two studies are carried out. In a first case, the velocity is applied in the x direction then this is applied in the y direction. DE calculations are performed using a time step of $1.815e^{-5}$s and stress fields are evaluated for a strain equal to $3.63e^{-4}$ corresponding to 20,000 time steps. In the present work, our choice is to determine the stress tensor at a mescoscopic scale using a tessellation of 1648 tetrahedra called specimens under the assumption that granular and continuous media produce identical internal and external forces. Thus, the average stress associated to each specimen of volume V and supposedly composed of a sufficient number of particles is written using tensorial notations as follows (Love-Weber formulation [17]):

$$\sigma_V^{ij} = \frac{1}{V} \sum_{j \in Z_i} f_{ij} d_{ij} \tag{2}$$

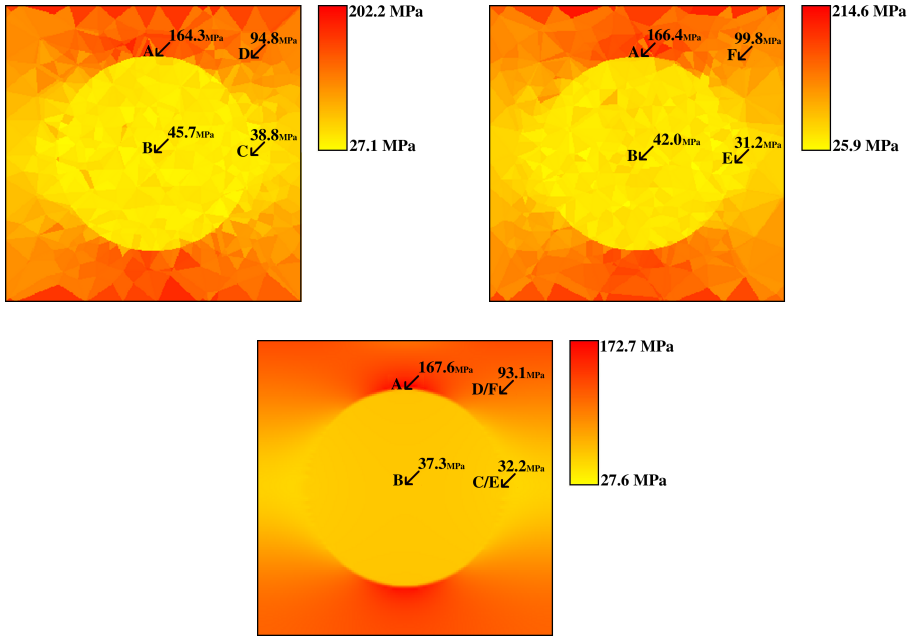

Figure 4: (a) σ_{xx} stress field with DE simulations (Cutting plane y=L/2), (b) σ_{yy} stress field with DE simulations (Cutting plane x=L/2) and (c) $\sigma_{xx/yy}$ stress field with FE simulations (Cutting plane x/y=L/2)

where f_{ij} is the cohesion force vector applied to the particle i by a particle j, d_{ij} is the relative position vector between particles i and j and Z_i is the set of particles located in the specimen. Figures 4a and b show σ_{xx} and σ_{yy} stress fields respectively obtained using the first and second loading case. From a qualitative standpoint, results are very similar and close to the Finite Element reference given in Figure 4c. Thus, whatever the configuration and the numerical approach, extremum values are located at top and bottom positions of the inclusion while minimum ones are located at both edges of the sphere. From a quantitative point of view, indicators are given at A(L/2,L/2,5L/6), B(L/2,L/2,L/2), C(5L/6,L/2,L/2), D(5/6,L/2,5L/6), E(L/2,5L/6,L/2) and F(L/2,5L/6,5L/6) positions. At A one, σ_{xx} and σ_{yy} stress values are respectively 164.3 MPa and 166.4 MPa and in quite good agreement with the FE prediction which is 167.6 MPa. At C and E positions, stress values given by the DE approach are respectively 38.8 MPa and 31.2 MPa and quite well conform the FE estimation of 32.2 MPa. All relative errors with respect to FE predictions are always less than 20% which exhibits the good adequation between FE and DE approaches.

3.1.2 Unidirectional fiber composite

The case of a 3D heterogeneous medium composed of a single metallic fiber drowned in a ceramic matrix is investigated. We consider the same elastic properties as previously used in the case of the spherical inclusion. The microstructure is modeled using a cubic pattern of length L=1cm composed of a single cylinder the axis of which is parallel to the y direction is generated. The radius of the cylinder is equal to one quarter of the length of the cube so that the volume fraction of the cylinder ϕ_C is theoretically equal to 0.196. First of all, a study is carried out in order to numerically determine ϕ_C and deduce it a suitable number of particles. We verify that a minimum number of 1,000,000 particles has to be handled in order to meet the theoretical ϕ_C value with a relative error less than 1%. DE calculations are carried out using a time step of $1.815e^{-5}$s and stress fields are determined using Equation 2 and a

tessellation of pentahedral specimens for a strain equal to 3.63e^{-4} corresponding to 20,000 time steps. Symmetric boundary conditions are handled and an imposed velocity of 1e^{-5} m/s is applied in the x direction. Figures 5a and b illustrate the σ_{xx} stress field in the cutting plane y=L/2 for DE and FE simulations respectively. For information purposes, the DE stress field is estimated using a tessellation of 3984 pentahedra. From a qualitative standpoint, stress fields are very similar with a maximum value located close to A position of coordinates (L/2,3L/4,L/2) and a minimum one located close to C position of coordinates (3L/4,L/2,L/2). From a quantitative standpoint, stress values extracted at A, B, C and D positions for the DE simulation are in quite good agreement with those given by the FE approach. Thus, relative errors with respect to FE estimations are close to 10%.

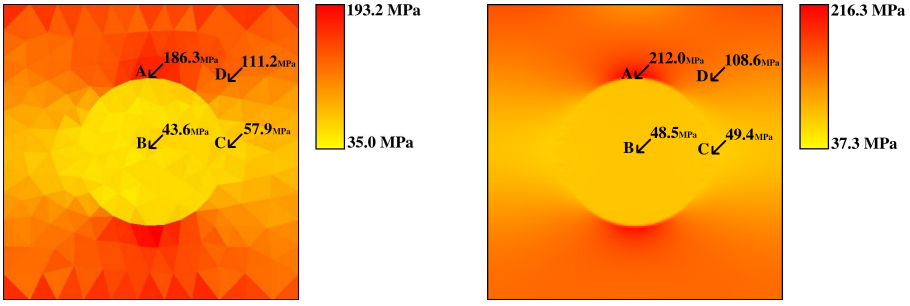

Figure 5: σ_{xx} stress field (a) Case of DE simulations and (b) Case of FE simulations (Cutting plane y=L/2)

3.2 Multi-fiber composite

We investigate the case of a multi-fiber composite composed of parallel metallic fibers embedded in an alumina matrix. Due to the symmetry of the material configuration, a 2D model is considered. A 2D square pattern of length L= 0.1m constituted of 25 monodisperse closely-packed fibers of radius R=9.6mm is generated using the LSA without periodicity assumptions. Thus, the compacity of the final packing is close to 0.73 due to wall effects. Figure 6 depicts the 2D square pattern. Elastic properties of each phase are those given in the previous subsection dedicated to single inclusion problems. Based on the works of Haddad et al., an ECD constituted of 100,000 particles is generated in order to ensure the representativity of each phase. Quasi-static tensile tests are set up. An outer displacement of 1.2e^{-5}m is imposed at both lateral edges of the square pattern in the x-direction and a time step of 1.6e^{-9}s is used for DE calculations. The ceramic phase is a brittle material the hydrostatic stress limit of which is supposed equal to 200 MPa. The metallic phase is supposed elastic with an infinite stress limit. Please notice that the current configuration leads to stress values lower than the stress limit of both phases so that no damaging occurs in the material.

In the present study, the hydrostatic stress σ_H is estimated at the scale of the particle using Zhou's formulation [15] which relates the equivalent stress tensor σ_i of a particle i to the internal cohesion forces as follows :

$$\sigma_i = \frac{1}{2\Omega_i} \sum_{j \in Z_i} \mathrm{f}_{ij} \mathrm{d}_{ij} \tag{3}$$

$$\sigma_H = \frac{\mathrm{Trace}(\sigma_i)}{2} \tag{4}$$

where f_{ij} is the cohesion force vector applied to the particle i by a particle j, d_{ij} is the relative position

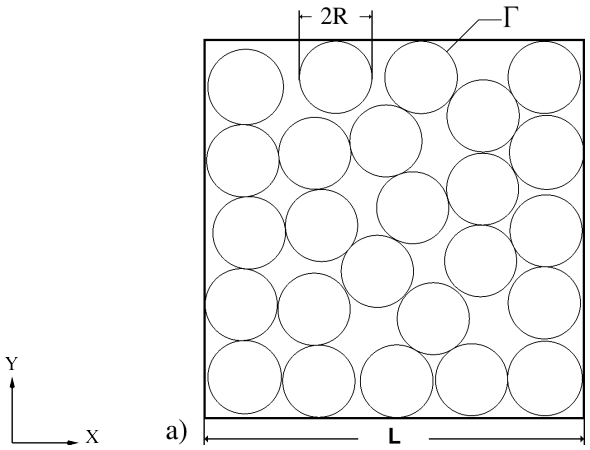

Figure 6: 2D square pattern of the closely-packed fiber composite

vector between particles i and j and Z_i is the set of particles linked to the particle i. Ω_i is the area of representation of the particle i which is approximated by the following expression :

$$\Omega_i = \frac{\mathrm{A}_i}{\phi} \tag{5}$$

where A_i is the real area of the particle and ϕ is the volume fraction of the granular system which is 0.85 in the present work where granular packings meet the assumptions of an RCP. Comparisons are done with FE results obtained using a mesh constituted of 491,000 nodes and 980,000 elements. Figures 7a and b show the hydrostatic stress field predicted using DE and FE calculations. From a quantitative standpoint, the DEM-based approach leads to a maximum stress higher than the one given by FE simulations, namely 128 MPa versus 85.7 MPa. However, the maximum value is located at the same position M of coordinates (90.4mm;20.6mm). Stress values are extracted from several positions of the square pattern. Table 1 provides the stress values predicted at A(21.1mm;39.3mm), B(62.6mm;70.5mm), C(40.3mm;88.6mm) and D(90.6mm;59.7mm) positions. Globally, DE predictions are in quite good agreement with FE ones except for the maximum value which is clearly overestimated in the case of DE calculations. These results exhibit the relevance of the DEM-based approach to predict the hydrostatic stress field in the present configuration of a material with a complex microstructure. Variability effects impact on the maximum value but its position is a priori not affected.

	A position	B position	C position	D position	Maximum value
DE predictions	18.4 MPa	14.6 MPa	-1.27 MPa	71.0 MPa	128 MPa
FE predictions	22.8 MPa	17.8 MPa	-1.03 MPa	60.7 MPa	85.7 MPa

Table 1: Hydrostatic stress values at A, B, C and D positions

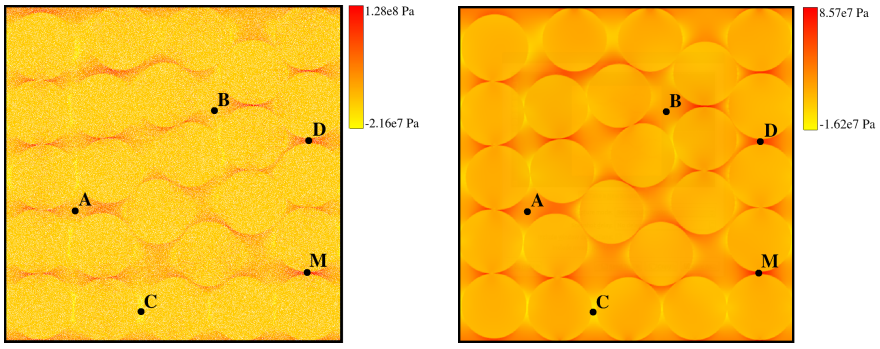

Figure 7: Hydrostatic stress field obtained using (a) DE calculations and (b) FE Calculations : case of the closely-packed fiber composite

4 Application to cracks initiation and propagation within a multi-fiber composite

4.1 Failure criterion

We consider the RDEF process [18] which is based on the deletion of a DE when a given stress criterion is reached. This choice is motivated by previous studies [11, 18] which highlighted the ability of such an approach to model complex crack patterns in homogeneous [18] and heterogeneous [11] media in comparison with the classical bond-based Rankine criterion. In the present work, we limit our studies to the brittle fracture of fragile materials such as silica and alumina with a mode I crack propagation but shear or mixed fracture mode could also be envisaged. In order to take into account the ability of fragile material to resist in compression, we assume a criterion based on the hydrostatic stress which is only positive for local tensile solicitations. Thus, the fracture occurs when the hydrostatic stress σ_H is greater than a given stress limit σ_{lim} :

$$\sigma_H \geq \sigma_{lim} \tag{6}$$

From a practical standpoint, when the criterion is reached, the particle i and its set of cohesive links are deleted.

4.2 Interfacial debonding

Interfacial debonding occuring at the interface Γ between two phases of a heterogeneous medium is simulated using DDZM [19]. During the simulation, some cohesive links connect two particles belonging to two different phases and consequently cross the interface Γ between two phases. The main idea consists in replacing the beam element by a spring-like one of normal stiffness K_n^Γ. In this model, the displacement u_n^Γ is related to the normal bonding force F_n^Γ as follows :

$$\mathrm{F}_n^\Gamma = \mathrm{K}_n^\Gamma \mathrm{u}_n^\Gamma \tag{7}$$

where u_n^Γ is the normal displacement of the spring element. Two regimes are considered : a linear elastic loading and an exponential softening one which are illustrated in Figure 8. In the first regime, when $\mathrm{u}_n^\Gamma < \mathrm{u}_n^{\Gamma,c}$ where $\mathrm{u}_n^{\Gamma,c}$ is the critical displacement, K_n^Γ is constant and equal to a given $\mathrm{K}_n^{\Gamma,0}$ stiffness:

$$\mathrm{K}_n^\Gamma \left(\mathrm{u}_n^\Gamma < \mathrm{u}_n^{\Gamma,c}\right) = \mathrm{K}_n^{\Gamma,0} \tag{8}$$

In the second regime, when $\mathrm{u}_n^\Gamma \geq \mathrm{u}_n^{\Gamma,c}$, K_n^Γ explicitly depends on u_n^Γ and $\mathrm{u}_n^{\Gamma,c}$ according to an exponential decrease so that K_n^Γ tends to zero for high displacements :

$$\mathrm{K}_n^\Gamma\left(\mathrm{u}_n^\Gamma \geq \mathrm{u}_n^{\Gamma,c}\right) = \frac{1}{exp\left(\dfrac{\mathrm{u}_n^\Gamma - \mathrm{u}_n^{\Gamma,c}}{\mathrm{u}_n^{\Gamma,c}}\right)}\mathrm{K}_n^{\Gamma,0} \tag{9}$$

From a practical standpoint, the normal stiffness K_n^Γ only depends on two parameters, namely the linear stiffness $\mathrm{K}_n^{\Gamma,0}$ and the critical displacement $\mathrm{u}_n^{\Gamma,c}$ which is a priori unknown. However, this latter can be determined knowing the interfacial stress limit σ_{lim}^Γ using the following relation :

$$\mathrm{u}_n^{\Gamma,c} = \frac{\sigma_{lim}^\Gamma \mathrm{A}_\Gamma}{\mathrm{K}_n^{\Gamma,0}} \tag{10}$$

where A_Γ is the area associated to the spring element which is chosen equal to A_μ.

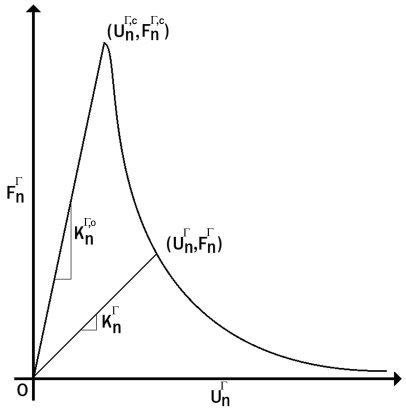

Figure 8: F_n^Γ-u_n^Γ relation

4.3 Application to the case of the multi-fiber composite

We consider the study case of the multi-fiber composite discussed in the previous section under the following hypotheses. Metallic and ceramic phases follow a linear elastic behavior with properties given in Table 2. We remind that the stress limit of the metal is assumed infinite so that no damage occurs within the fiber. Thus, the sole rupture of the alumina matrix is taken into account in our model. We consider the RDEF criterion based on the hydrostatic stress field evaluated at the scale of the particle. The behavior of the interface Γ is described by the DDZM and spring-like elements the normal stiffness $\mathrm{K}_n^{\Gamma,0}$ of which are chosen equal to the geometric average of normal stiffnesses K_n^f and K_n^m associated to the fiber and the matrix:

$$\mathrm{K}_n^{\Gamma,0} = \sqrt{\mathrm{K}_n^f \mathrm{K}_n^m} \tag{11}$$

The macroscopic interfacial stress limit σ_{lim}^Γ is defined as a ratio C_Γ of the matrix stress limit σ_{lim}^m so that :

$$\sigma_{lim}^\Gamma = \mathrm{C}_\Gamma \sigma_{lim}^m \tag{12}$$

A quasi-static tensile test is simulated up to the sample break by applying a velocity of 0.1 $\mathrm{m.s}^{-1}$ at both

Material	Alumina	Metal
Young's modulus (GPa)	350	70
Poisson's ratio	0.25	0.3
Density (kg/m^3)	3,900	2,700
σ_{lim} (MPa)	200	∞

Table 2: Properties of each phase

lateral edges of pattern in the x-direction. C_Γ is set to 0.25 so that the interfacial debonding is prone to arise before cracking. DE simulations are carried out using an initial time step of 1.6e^{-9}s. Figures 9a, b and c show the hydrostatic stress field and the interfacial debonding at three given times t=1.33e^{-4}s, t=1.44e^{-4}s and t=1.60e^{-4}s. In a first step, the interfacial debonding appears at a position of coordinates (54.4mm;18.2mm) which is encircled in blue on Figure 9a. Then, the debonding propagates vertically from fiber to fiber throughout the contact points. The maximum hydrostatic stress is 4.32e^8 Pa which is higher than the failure criterion. However, no matrix rupture occurs except for local points since hot spots are in fact located on the debonded interface. Finally, the debonding area reaches the edges of the square pattern and the ruin of the material starts. These findings are in good agreement with a C_Γ ratio less than 1 for which the debonding is predominent. Besides, as expected, the fibre-matrix debonding propagates in the perpendicular direction of the tensile solicitation.

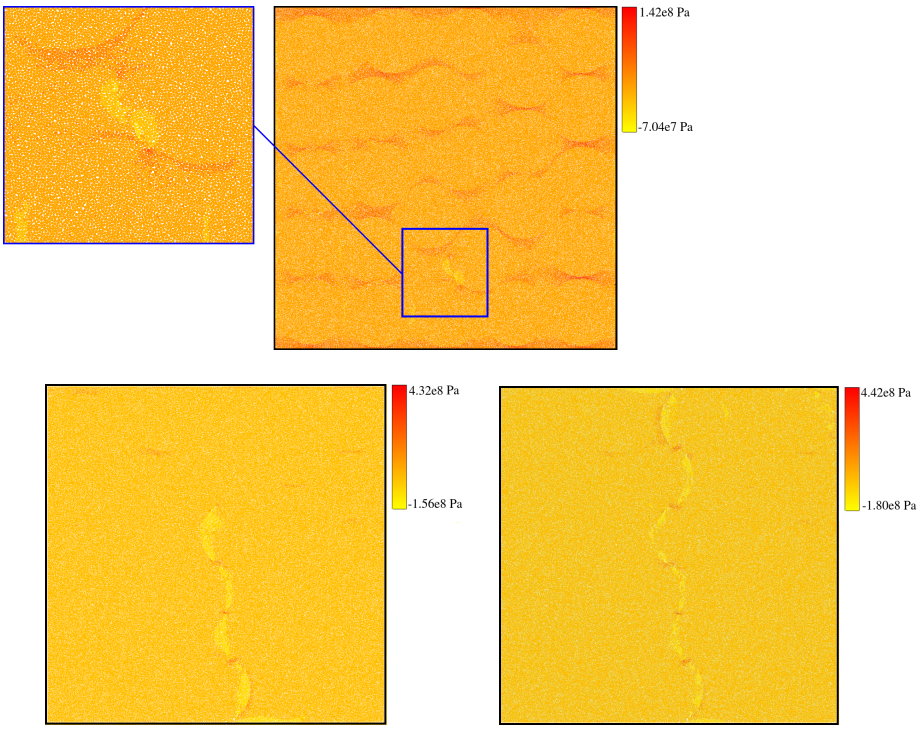

Figure 9: Hydrostatic stress field and interfacial debonding within the closely-packed fibre composite at time (a) t=1.33e^{-4}s, (b) t=1.44e^{-4}s and (c) t=1.60e^{-4}s

5 Conclusions and prospects

The present work was dedicated to a DEM-based approach to simulate the mechanical behavior of heterogeneous media. Results exhibited the relevance of this approach to yield the elastic response of the medium in the context of single inclusion problems and a multi-fiber composite. From a quantitative standpoint, comparisons in terms of stress field showed a good agreement with the FEM. These also highlighted some differences since a discrete approach is prone to local variabilities which are only diminished by using a tessellation of specimens. Besides, the issue of cracks initiation and propagation was investigated in the context of a multi-fiber composite. This study showed realistic crack patterns as well as a good location of the crack initiation. These results are encouraging and open up some interesting prospects. Thus, we are currently working on non-linear mechanical behaviors and the thermomechanical coupling based on a dilatation model. We also envisage to investigate and quantify the local fluctuation of properties in order to better control this phenomenon and consider realistic variabilities in the mechanical simulation.

References

[1] P.A. Cundall, O.D.L. Strack, Discrete numerical model for granular assemblies, Géotechnique, 29 (1979) 47–65.

[2] P.W. Cleary, C.S. Campbell, Self-lubrication for long run-out landslides: examination by computer simulation, Journal of Geophysical Research, 98(B12) (1993) 21911–24.

[3] H. Ben Dhia, G. Rateau, The Arlequin method as a flexible engineering design tool, International Journal for Numerical Methods in Engineering, 62 (2005) 1442–1462.

[4] M. Jebahi, D. André, F. Dau, J.L. Charles, I. Iordanoff, Simulation of Vickers indentation of silica glass, Journal of Non-Crystalline Solids, 378 (2013) 15–24.

[5] S. Hentz, F.V. Donzé, L. Daudeville, Discrete element modelling of concrete submitted to dynamic loading at high strain rates, Computers & Structures, 82(29-30) (2004) 2509–2524.

[6] Y. Tan Y, D. Yang, Y. Sheng, Discrete element modelling of fracture and damage in the machining of polycristalline SiC, Journal of the European Ceramic Society, 29(6) (2009) 1029–1037.

[7] E. Schlangen, E.J. Garboczi, Fracture simulations of concrete using lattice models : Computational aspects, Engineering Fracture Mechanics, 57(2) 1997 319–332.

[8] D. André, I. Iordanoff, J.C. Charles, J. Neauport, Discrete element method to simulate continuous material by using the cohesive beam model, Computer Methods in Applied Mechanics and Engineering, 213 (2012) 113–128.

[9] R. Kumar, S. Rommel, D. Jauffrès, P. Lhuissier, C. Martin, Effect of packing characteristics on the discrete element simulation of elasticity and buckling, International Journal of Mechanical Sciences, 110 (2016) 14–21.

[10] H. Haddad, W. Leclerc, M. Guessasma, Application of DEM to predict the elastic behavior of particulate composite materials, Granular Matter, 17 (2015) 459–473.

[11] L. Maheo, F. Dau, D. André, J.L. Charles, I. Iordanoff, A promising way to model cracks in composite using Discrete Element Method, Composites Part B, 71 (2015) 193–202.

[12] B.D. Le, F. Dau, J.L. Charles, I. Iordanoff, Modeling damages and cracks growth in composite with a 3D discrete element method, Composites Part B, 91 (2016) 615–630.

[13] B.D. Lubachevsky, F.H. Stillinger, Geometric properties of random disk packings, Journal of Statistical Physics, 60 (1990) 561–583.

[14] A. Donev, I. Cisse, D. Sachs, E.A. Variano, F.H. Stillinger, R. Connelly, et al., Improving the density of jammed disordered packings using ellipsoids, Science, 303 (2004) 990–993.

[15] M. Zhou, A new look at the atomic level virial stress : on continuum-molecular system equivalence, Proceedings of the Royal Society of London, Mathematical, Physical and Engineering Sciences, 2037 (2003) 2347–2392.

[16] F. Nicot, N. Hadda, M. Guessasma, J. Fortin, O. Millet, On the definition of the stress tensor in granular media, International Journal of Solids and Structures, 50 (2013) 2508–2517.

[17] A.E.H. Love, A treatise of mathematical theory of elasticity, Cambridge University Presse, Cambridge, 1927.

[18] D. André, M. Jebahi, I. Iordanoff, J.L. Charles, J. Neauport, Using the discrete element method to simulate brittle fracture in the indentation of a silica glass with a blunt indenter, Computer Methods in Applied Mechanics and Engineering, 265 (2013) 136–147.

[19] X. Liu, R. Duddu, H. Waisman, Discrete damage zone model for fracture initiation and propagation, Engineering Fracture Mechanics, 92 (2012) 1–18.